2

PERMANENT GROUND DEFORMATION HAZARDS

The principal forms of permanent ground deformation (PGD) are surface faulting, landsliding, seismic settlement and lateral spreading due to soil liquefaction. Whether the buried pipeline fails when subjected to PGD depends, in part, on the amount and spatial extent of the PGD, which are introduced here.

The aim of this chapter is to provide a general overview of permanent ground deformation. First, we discuss the types of faults and the expected amount of fault offset, which is empirically correlated with earthquake magnitude. Second, we describe the types of landslides, empirical relations for the occurrence of landslides, and analytical relations for the amount of earth flow movement. Third, two approaches to evaluate ground settlement induced by soil liquefaction are introduced. Finally, we present the characteristics of lateral spreads induced by soil liquefaction.

2.1 FAULT

An active fault is a discontinuity between two portions of the earth crust along which relative movements can occur. The movement is concentrated in relatively narrow fault zones. Principal types of fault movement include strike-slip, normal-slip and reverse slip as shown in Figure 2.1. In a strike-slip fault the predominant motion is horizontal, which deforms a continuous pipe primarily in tension or compression depending on the pipe-fault intersectional angle. In normal and reverse faults the predominant ground displacement is vertical. When the overhanging side of the fault moves downwards, the fault is normal, which deforms a horizontal pipe primarily in tension. When the overhanging side of the fault moves upwards, the fault is reverse, which deforms a horizontal pipe primarily in compression.

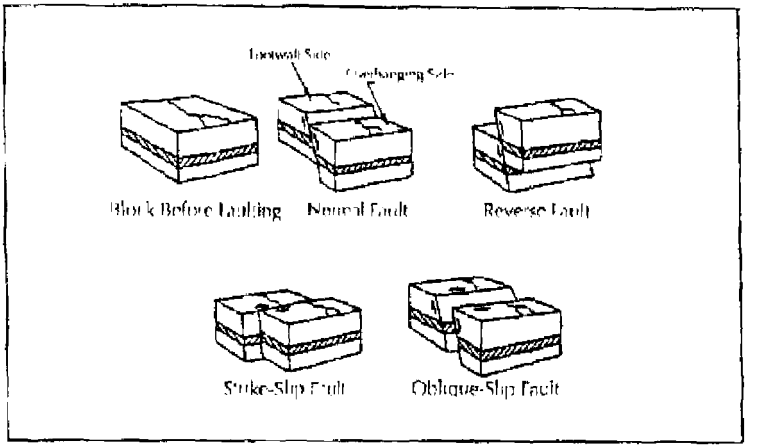

After Meyerson, 1991

■ Figure 2.1 Block Diagrams of Surface Faulting

As mentioned previously in Section 1.2, the strain in a continuous pipe subject to fault offset depends on the amount of the fault offset and the pipe-fault intersectional angle. Here we only discuss the amount of fault offset. The effects of the intersectional angle will be discussed in Chapter 8.

Various empirical relations between fault displacement and moment magnitude have been proposed. They all have a similar logarithmic form. Here we only introduce the relationship by Wells and Coppersmith (1994) because it extends previous studies by including data from recent earthquakes and from new investigations of older earthquakes. Based on a worldwide data base of 421 historical earthquakes, Wells and Coppersmith selected 244 earthquakes, and developed the following empirical relationships:

$$\log\delta_r = -6.32 + 0.90M \text{ for Strike-Slip Fault} \qquad (2.1)$$

$$\log\delta_r = -4.45 + 0.63M \text{ for Normal Fault} \qquad (2.2)$$

$$\log\delta_r = -0.74 + 0.08M \text{ for Reverse Fault} \qquad (2.3)$$

where δ_r is the average fault displacement, in meters, M is the moment magnitude. The observed fault displacement in the Wells and Coppersmith's data base (i.e., magnitude range from 5.6 to 8.1) varies from 0.05 to 8.0 m for strike-slip faults, 0.08 to 2.1 m for normal faults, and 0.06 to 1.5 m for reverse faults as shown in Figure 2.2. The maximum fault displacement is twice the average fault displacement, according to Wells and Coppersmith. Note that the single curve (i.e., solid lines) in Figure 2.2(a) is for a combined model, while the three curves in Figure 2.2 (b) are for strike slip, reverse and normal faults respectively.

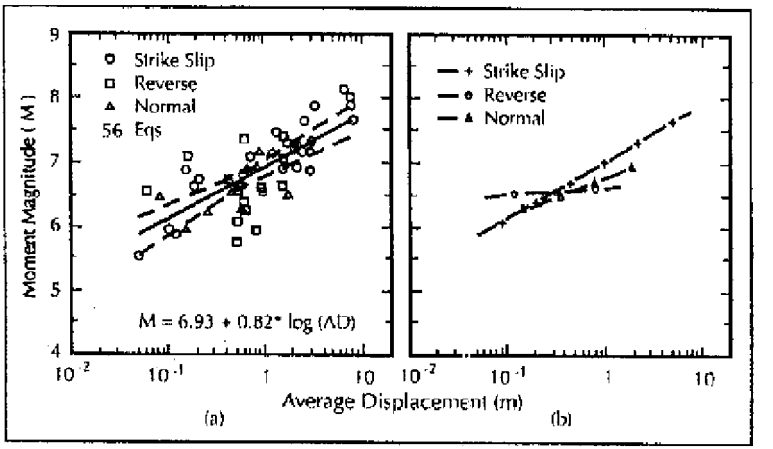

After Wells and Coppersmith, 1994

■ **Figure 2.2 Regression of Average Surface Displacement on Magnitude**

If a fault is poorly known or blind (i.e., lack of clear surface expression to judge fault type), the all-slip-type regression provided by Wells and Coppersmith can be used to evaluate the expected fault displacement.

$$\log\delta_r = -4.80 + 0.69M \text{ for all} \qquad (2.4)$$

2.2 LANDSLIDE

Landslides are mass movements of the ground which may be triggered by seismic shaking. A large number of systems have been developed to classify landslides. The most widely used classification system in the United States was devised by Varnes (1978). Varnes identified five principal categories based on soil movements, geometry of the slide, and the types of material involved. Varnes's categories are: falls, topples, slides, spreads, and flows. Herein, lateral spreading is considered to be a liquefaction-induced phenomenon, and is discussed in Section 2.3.

Based on the different effects on pipelines, Meyersohn (1991) established three types of landslides as shown in Figure 2.3.

As shown in Figure 2.3, Type I includes rock fall and rock topple, which can cause damage to above-ground pipelines by direct impact of falling rocks. This type of landslide has relatively little effect on buried pipelines and will not be discussed in detail. Type II includes earth flow and debris flow, in which the transported material behaves as a viscous fluid. Large movements (several meters or more) are often associated with this type of landslide but the expected amount of movement is difficult to predict. Type II landslides will not be discussed herein. Type III includes earth slump and earth slide, in which the earth moves, more or less as a block. They usually develop along natural slopes, river channels, and embankments. Because pipelines often cross such zones, the following will focus on this type of landslide.

Empirical methods have been used to determine upper bounds for the occurrence of landslides. Figure 2.4 shows one such relation (Applied Technology Council, 1985), in which the maximum distance of observed landslides to the fault rupture zone is plotted as a function of earthquake magnitude.

Recent work by Jibson and Keefer (1993) resulted in analytical estimation of the expected amount of landslide movement. They used the computer program STABL (Siegel, 1978) to search for the critical failure surface by randomly generating slip surfaces and calculating the factor of safety (FS). The factor of safety is the ratio

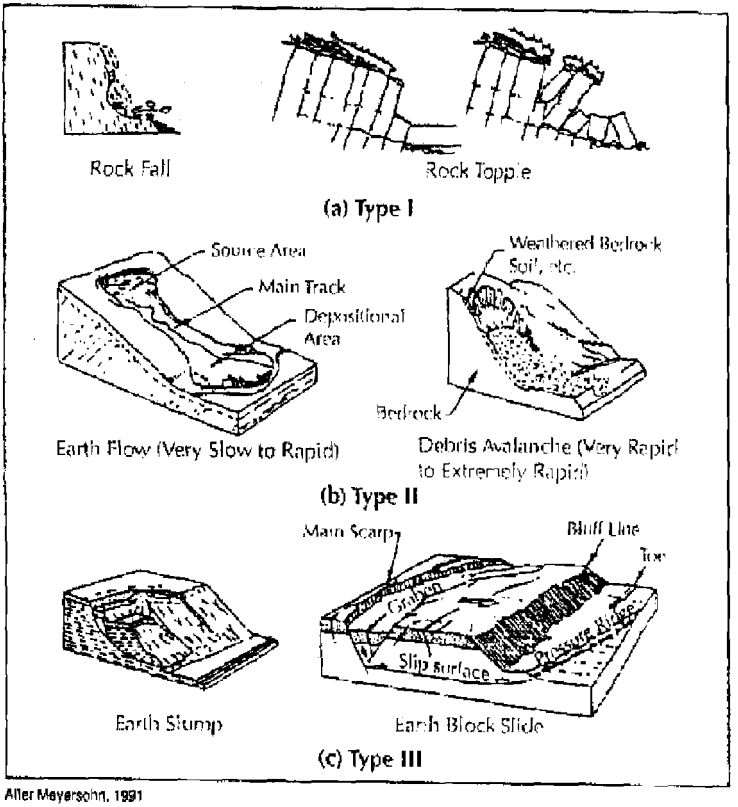

After Meyerson, 1991

■ Figure 2.3 Selected Ground Failure Associated with Landsliding

of the sum of the resisting forces and sum of the driving forces that tend to cause movement. That is, the critical failure surface is the slip surface with the lowest factor of safety.

Based on Newmark's Block model (Newmark, 1965), the critical acceleration, a_c, can then be defined as:

$$a_c = g(FS \quad 1)\sin\alpha \qquad (2.5)$$

where g is the acceleration due to gravity and α is the inclined angle of the slope.

The displacement of the block is then calculated by double integration of the ground accelerations larger than the critical acceleration a_c.

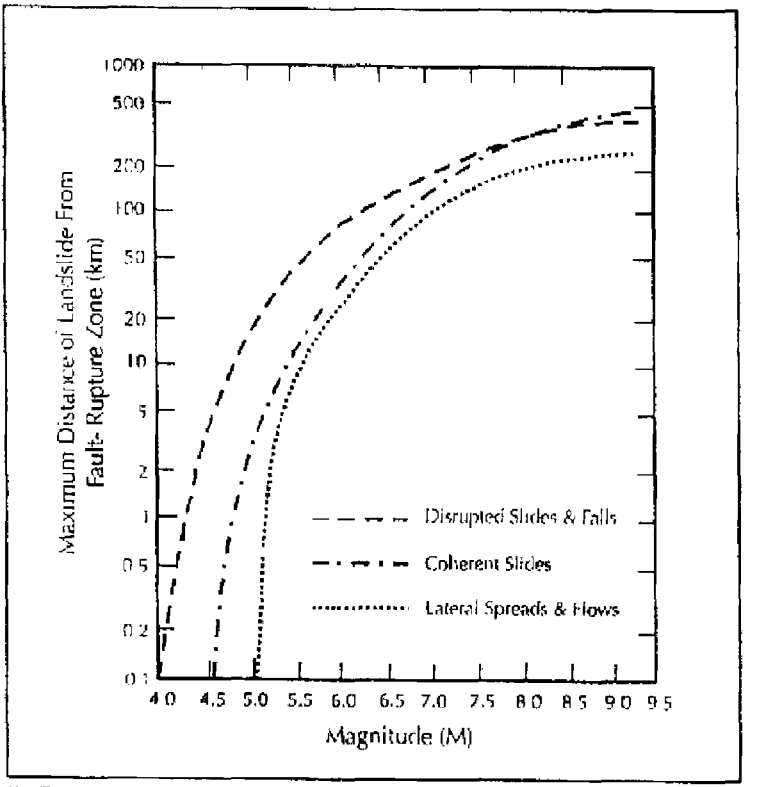

After ATC-13, 1985

■ Figure 2.4 Occurrence of Landslide vs. Magnitude of Earthquake

Jibson and Keefer selected 11 strong-motion records to estimate the Newmark displacement. For each of the strong-motion records, they calculated the Newmark displacement for several critical accelerations between 0.02 and 0.4 g, which is considered to be the practical range of interest for most earthquake-induced landslides. The resulting data are plotted in Figure 2.5, for which the best regression function is:

$$\log D_N = 1.460 \log I_a - 6.642 a_c + 1.546 \qquad (2.6)$$

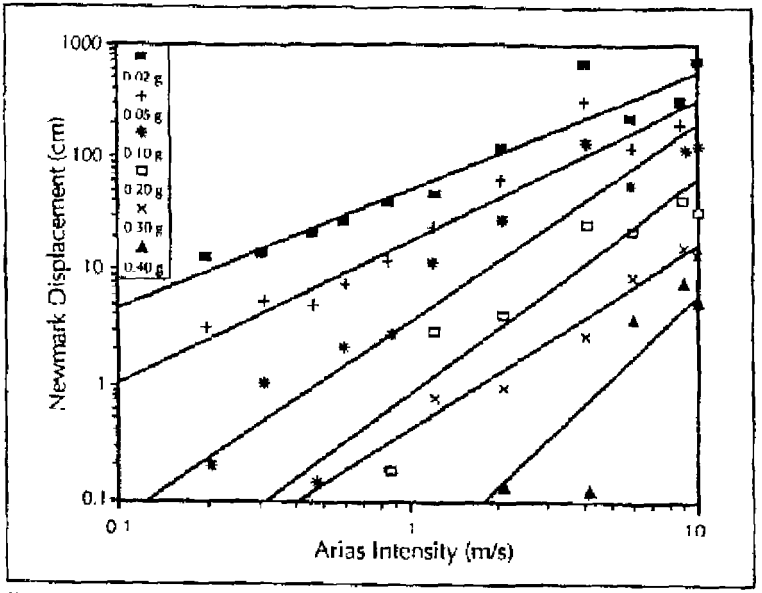

After Jibson and Keefer, 1993

Figure 2.5 Newmark Displacement vs. Arias Intensity for Critical Accelerations of 0.02-0.40g

where D_N is the Newmark displacement in centimeters and I_a is the Arias intensity in g's, defined as:

$$I_a = \frac{\pi}{2g} \int [a(t)]^2 dt \qquad (2.7)$$

where $a(t)$ is the ground acceleration time history

In this regard, Wilson and Keefer (1983) developed a simple relationship between Arias intensity, earthquake magnitude, M, and source distance, R, in kilometers:

$$\log I_a = M - 2\log R - 4.1 \qquad (2.8)$$

Note that Equation 2.8 is developed from California earthquakes and may slightly underestimate shaking intensity in the central United States.

2.3 LATERAL SPREADING

Lateral spreads develop when a loose saturated sandy soil deposit is liquefied due to seismic shaking. Liquefaction causes the soil to lose its shear strength, which in turn results in the flow or lateral movement of liquefied soil. Although the ground movement is primarily horizontal, Towhata et al. (1991) observed that vertical soil movement often accompanies liquefaction-induced lateral spreading. However, the vertical component is typically small and will be disregarded herein.

In terms of pipeline response, two situations are possible. In the first case such as at the Ogata Primary School site during the 1964 Niigata event, the top surface of the liquefied layer is essentially at the ground surface. For this first case, a pipeline is subject to horizontal force due to liquefied soil flow over and around the pipeline, as well as uplift or buoyancy forces. In the second case such as at the Mission Creek site during the 1906 San Francisco event, the top surface of the liquefied layer is located below the bottom of a typical pipeline. That is, the pipeline is contained in a non-liquefied surface soil layer which rides over the liquefied layer. For this second case, the pipeline is subject to horizontal forces due to non-liquefied soil-structure interaction but not subject to buoyancy effects. Pipeline response to such horizontal loading is discussed in Chapter 6 and 7. Pipeline response to buoyancy forces is discussed in Chapter 7.

The direction of movement for the lateral spread is controlled by geometry. When the lateral spread occurs at or near a free face, the movement is generally towards the free face. When the lateral spread occurs away from a free face, the movement is down the slope of the ground surface or down the slope of the bottom of the liquefied layer. For the "PGD towards a free face" data, the observed distance is from 10 to 300 m (33 to 984 ft) away from the free face with average value of 100 m (Bartlett and Youd, 1992). For the "PGD away from a free face" data, the observed slope is from 0.1% to 6% with an average value of 0.55%.

There are four geometric characteristics of a lateral spread which influence pipeline response in a horizontal plane. With ref-

erence to Figure 2 6, these are the amount of PGD movement δ, the transverse width of the PGD zone W, the longitudinal length of the PGD zone L, and the pattern or distribution of ground movement across and along the zone.

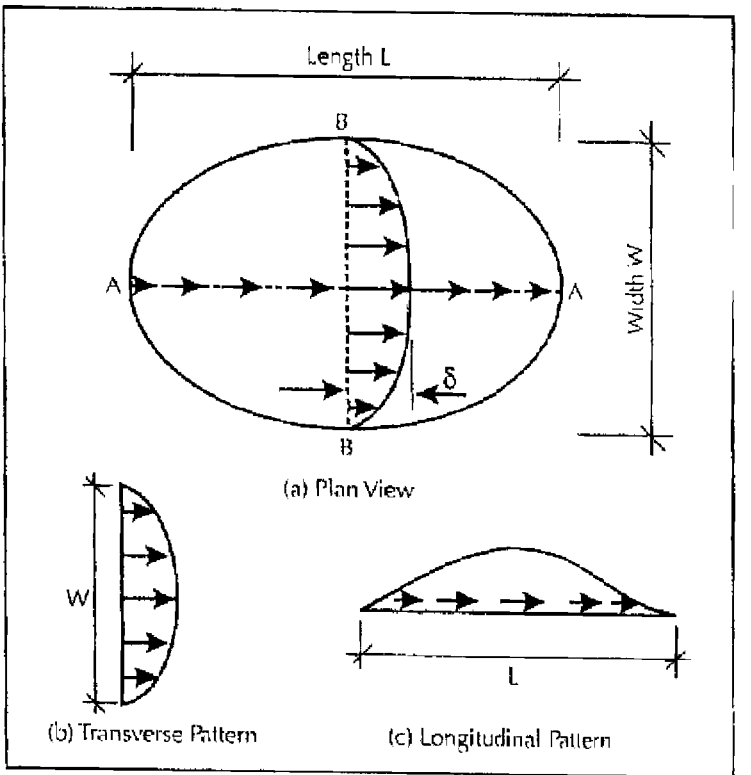

■ Figure 2 6 Characteristics of a Lateral Spread

In the following subsection, available information which can be used to quantity each of these characteristics is presented.

2.3.1 AMOUNT OF PGD

In general, the potential for PGD to induce pipe damage is related to the amount of ground movement, the length and width of the PGD zone as well as the pattern of deformation. Predicting the amount of ground displacement due to soil liquefaction is a

challenging problem. Nevertheless there have been a number of studies, both analytical and empirical, which have addressed this issue. These studies are reviewed below.

Analytical and Numerical Models

Dobry and Baziar (1990), and Mabey (1992) estimate liquefaction-induced displacement using a Newmark sliding block analysis. In this analysis a 1-D, rigid soil block model is allowed to displace along a planar failure surface during time intervals when the sum of the inertial (i.e., earthquake) and gravity (i.e., self weight) components along the slide surface exceeds the shear strength of the soil.

Hamada et al. (1987), Towhata et al. (1991), and Yasuda et al. (1991) used 2-D, static elastic models to estimate the amount of lateral spreading displacement. They model the non-liquefied surface layer as a 2-D, elastic beam, floating on the liquefied layer below, and subject to lateral loading (the component of the gravity load parallel to the inclined ground surface). An analytical, closed form solution is used to calculate the ground displacement by minimizing the potential energy of the system.

Orense and Towhata (1992) used a variational principle to develop a 3-D analytical relation for the amount of liquefaction-induced ground displacement. The method is based on the principle of minimum potential energy. The lateral displacements are calculated based on the assumption on a half sinusoidal distribution of lateral displacement along a vertical section (i.e., zero at the bottom and maximum at the top) and vertical displacements are calculated based on constant volume assumption. The Rayleigh-Ritz method is employed to obtain the solution.

However, as pointed out by Bartlett and Youd (1992), these analytical and numerical models have not been applied to a wide range of earthquake and site conditions. More validation and calibration studies are likely needed before these analytical and numerical techniques can be used directly by practicing engineers.

Empirical Model

Several empirical models have been proposed to predict lateral spread displacements. The following brief review describes

these existing empirical relations, their underlaying assumptions and expected range of applicability.

Work by Hamada et al. (1986) suggests that the amount of PGD induced by liquefaction is closely related to the geometric configuration of the estimated liquefied layer They proposed the following regression formula for the magnitude of horizontal PGD, δ, in meters:

$$\delta = 0.75\sqrt{h}\sqrt[3]{\theta_g} \qquad (2.9)$$

where h is the thickness of the liquefied layers, in meters, and θ_g is the slope of the lower boundary of the liquefied layer or the ground surface (%), whichever is larger.

Note that the Hamada et al. relation does not distinguish between the amount of expected PGD at a free face as opposed to that for gently sloping ground. In addition, the thickness of the liquefied layer is in a sense a pseudo parameter which accounts for the amount of ground shaking (related to earthquake magnitude and distance) as well as the soil characteristics at the site According to Bartlett and Youd (1992), it produces reasonable estimate for earthquakes with magnitude around 7.5 and epicenter distance in the 20 to 30 km range.

Youd and Perkins (1987) introduced the concept of a Liquefaction Severity Index (LSI) which is defined as the amount of PGD, in inches, associated with lateral spreading on gently sloping ground and poor soil conditions. LSI is arbitrarily truncated at 100. Youd and Perkins established a correlation between LSI, earthquake magnitude and distance for the western U.S. as follows:

$$\log LSI = -3.49 - 1.86\log R_d + 0.98M_w \qquad (2.10)$$

where R_d is the distance from the epicenter to the site, in kilometers for western U.S. earthquakes, and M_w is the earthquake magnitude.

Using that correlation as a starting point and data available for the 1811-12 New Madrid earthquakes, Turner and Youd (1987) proposed the following relation for the New Madrid area:

$$\log LSI = 4.252 - 1.276\log R_d \qquad (2.11)$$

Two separate equations are provided to account for differences in attenuation of strong ground motion east and west of the Rocky Mountains. Note that LSI given above is not a function of local soil parameters (i e , applies to the worst possible soil condition) nor ground slope (it applies to ground slopes between 0 5 and 5%). In addition, as with Hamada's work, the LSI relation does not distinguish between the expected amount of PGD at a free face as opposed to that for gently sloping ground condition.

Using data from 1906 San Francisco, 1964 Alaska, 1964 Niigata, 1971 San Fernando, 1979 Imperial Valley, 1983 Nihonkai-Chubu, 1983 Borah Peak and 1987 Superstition Hills earthquakes, Bartlett and Youd (1992) recently developed two empirical relations for the expected amount of PGD due to liquefaction The first is for lateral spreads down gentle ground slopes and the other is for lateral spreads at a free face.

For gently sloping ground condition, the relation is:

$$\log(\delta + 0.01) = -15.787 + 1.178M - 0.927 \log R_d - 0.013R_d + 0.429 \log S + 0.348 \log T_{15} + 4.527 \log(100 - F_{15}) - 0.922D_{50_{15}} \quad (2.12)$$

For PGD at a free face

$$\log(\delta + 0.01) = -15.787 + 1.178M - 0.927 \log R_d - 0.013R_d + 0.429 \log Y + 0.348 \log T_{15} + 4.527 \log(100 - F_{15}) - 0.922D_{50_{15}} \quad (2.13)$$

where δ is the permanent horizontal displacement of ground (m), M is the earthquake magnitude, R_d is the epicentral distance (km), S is the ground slopes (in percent, shown in Figure 2.7(a)), Y is the free face ratio (in percent, shown in Figure 2.7 (b)), F_{15} is the average fines contents in T_{15} (%), $D_{50_{15}}$ is the mean grain size in T_{15} (mm) and T_{15} is the thickness of saturated cohesionless soils with a corrected SPT value less than 15, (m).

Both equations include the effects of shaking at the site, soil properties and site topography. For a given amount of ground shaking (i.e., magnitude and epicenter distance fixed), the parameters

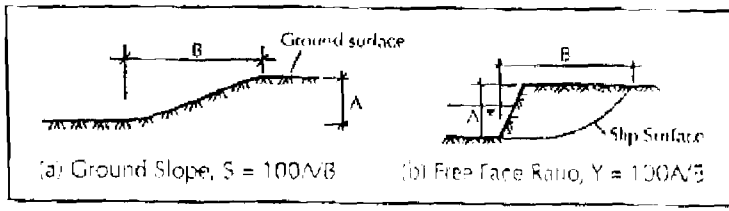

■ Figure 2.7 Elevation View Showing Ground Slope and Free Face Ratio

which most strongly influence the amount of PGD are the average fines contents, followed by the mean grain size and the ground slope/free face ratio. The accuracy of the Bartlett and Youd (1992) empirical relations are relatively good, in that predicted values are generally within a factor of two of the observed values. As such, they are arguably the best currently available relations for use in the western U.S.

2.3.2 Spatial Extent of Lateral Spread Zone

As will be seen later, the width and the length of the PGD zone have a strong influence on pipe response to PGD. Unfortunately the currently available information on the spatial extent of lateral spread zone is somewhat limited. Although one expects that the spatial extent of the lateral spread zone strongly correlates with the plan dimensions at the area which liquefied, analytical or empirical relations are not currently available. In the following, both the width W and length L as shown in Figure 2.6 will be discussed.

Information on observed values for the spatial extent of the lateral spread zone has been developed by Suzuki and Masuda (1991). Using data from the 1964 Niigata and 1983 Nihonkai-Chubu earthquakes, they presented scattergrams in Figure 2.8 of the amount of ground movement and spatial extent of the lateral spread zone for PGD away from a free face. Note that most all the observed widths are distributed in the range of about 80 to 600 m (262 to 1968 ft) and the lateral displacement tends to increase with increasing width.

In terms of the length of the lateral spread zone at a free face, the study by Bartlett and Youd (1992) provides useful information.

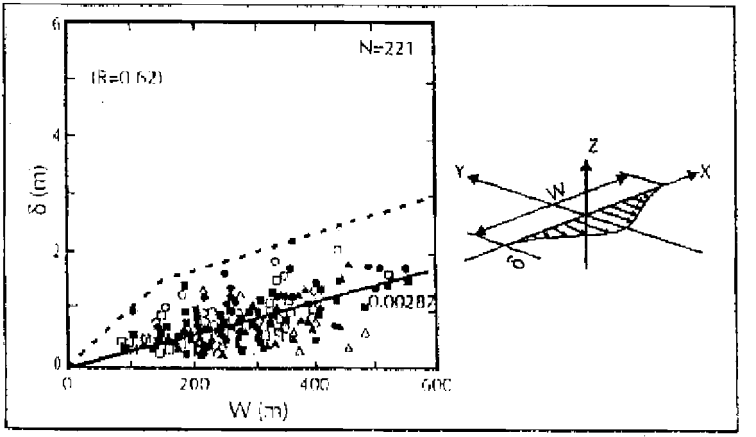

After Suzuki and Masuda, 1991

■ Figure 2.8 Observed Data on the Amount of PGD and the Width of the Lateral Spread Zone Away From a Free Face

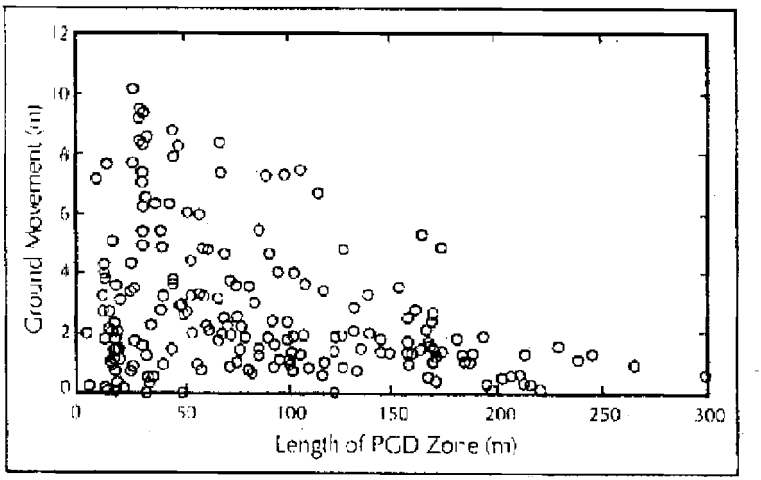

After Bartlett and Youd, 1992

■ Figure 2.9 Observed Data on the Amount of PGD and the Length of the Lateral Spread Zone at a Free Face

Figure 2.9 shows observed data on the amount of PGD and the length of the lateral spread zone at a free face. As with the observed PGD zone width shown in Figure 2.8, the observed lengths in Figure 2.9 are less than about 400 m (1312 ft), with most of the values below 200 m (656 ft). Although there is a large amount of scatter, the ground displacement appears to be a decreasing function of the length of the lateral spread zone for this free face situation. On the other hand, as discussed in relation to Figure 2.8, the ground displacement appears to be an increasing function of the width of the lateral spread zone for gently sloping ground situations.

Nevertheless, due to the large amount of scatter in these figures, it seems that the expected length and width of a lateral spread zone, particularly for site specific studies, should be based upon the expected plan area of liquefaction as opposed to the estimated ground movement.

2.3.3 PGD Pattern

As noted previously, the response of buried pipelines to PGD is influenced by the pattern of deformation, that is the variation of permanent ground displacement across the width (Figure 2.6(b)) or along the length (Figure 2.6(c)) of the lateral spread zone. The study by Hamada et al (1986) of liquefaction in the 1964 Niigata earthquake and 1983 Nihonkai-Chubu earthquake provide a wealth of information on observed longitudinal PGD patterns. Figure 2.10 shows longitudinal PGD observed along five of 27 lines in Noshiro City resulting from the 1983 Nihonkai-Chubu earthquake. In this figure the height of the vertical line is proportional to the observed horizontal PGD at the point.

Note that about 20% of the observed patterns (6 out of 27) have the same general shape as Figure 2.10(a). That is, they show relatively uniform PGD movement over the whole length of the lateral spread zone. The response of continuous buried pipeline to idealizations of these longitudinal patterns of PGD is discussed in Chapter 6.

Information on transverse patterns of PGD, as shown in Figure 2.6(b) is more limited. Figure 2.11 shows five transverse PGD patterns observed in the 1971 San Fernando earthquake and 1964 Niigata earthquake

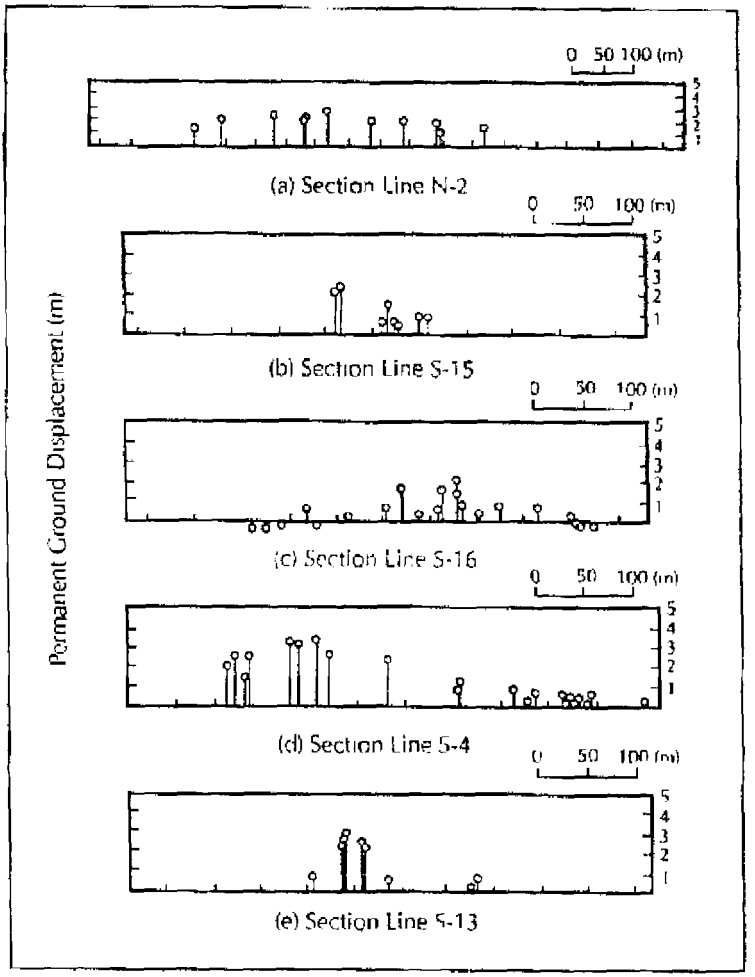

After Hamada et al. 1986

■ **Figure 2.10 Observed Ground Deformation**

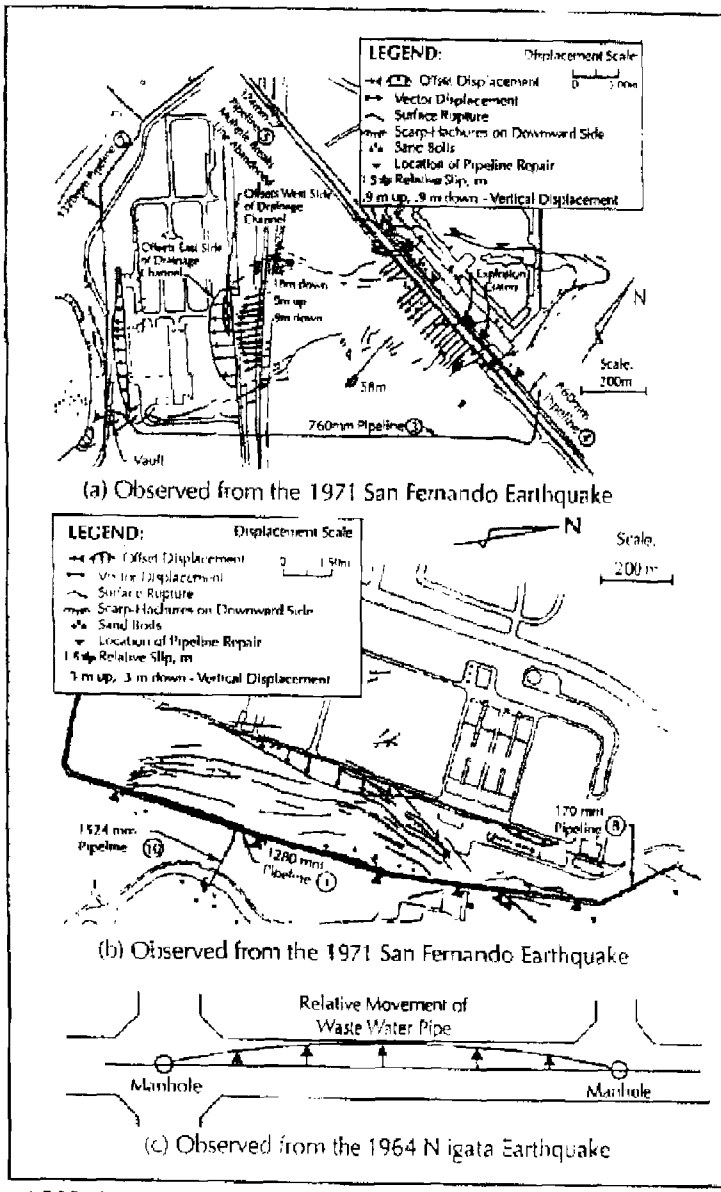

a, b O'Rourke and Tawfik 1983; c Hamada and T O'Rourke 1992

■ **Figure 2.11 Observed Transverse PGD Patterns**

SEISMIC SETTLEMENT

Earthquake induced subsidence may be caused by densification of dry sand, consolidation of clay or consolidation of liquefied soil. Among these three types, the liquefaction-induced ground settlement is somewhat more important in that it can lead to larger ground movement and hence higher potential for damage to buried pipeline system. Ground settlement induced by soil liquefaction is discussed below.

An example of observed seismic settlement due to liquefaction is shown in Figure 2.12. This figure presents contours of ground settlement in the Marina District occasioned by the 1989 Loma Prieta earthquake (T. O'Rourke et al., 1991).

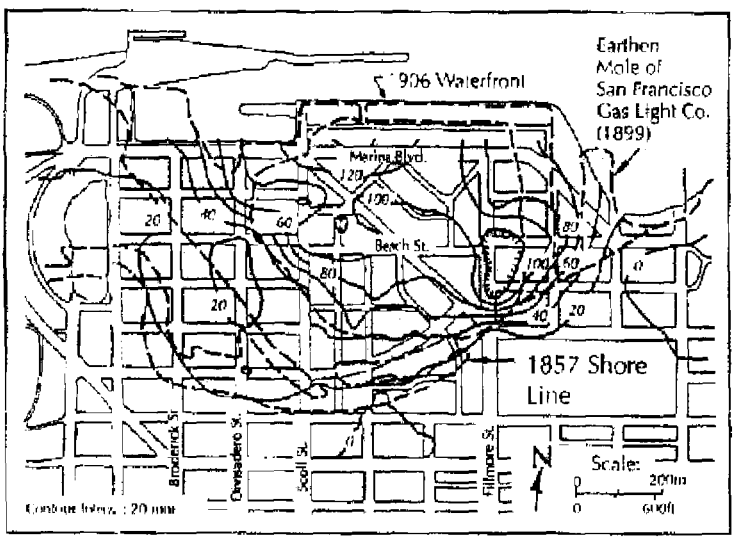

After T. O'Rourke et al., 1991

■ **Figure 2.12 Contour of Ground Settlement in Marina District**

Note that the maximum ground settlement is about 140 mm (5.5 in). In comparison to the expected amount of lateral spread deformation discussed previously, the expected amount of ground settlement, for the same general level of ground shaking, are typically smaller.

For saturated sands without lateral spread movement, Tokimatsu and Seed (1987) developed an analytical procedure to evaluate ground settlement. The fundamental relation is:

$$\delta = \sum (\varepsilon_v)_i h_i \qquad i = 1, 2, \ldots, n \tag{2.14}$$

where ε_v is the volumetric strain for a saturated sandy soil layer, h is the layer thickness and n is the number of sand layers with different SPT N-values.

The volumetric strain in each layer depends on the SPT N-value and the cyclic stress ratio as shown in Figure 2.13, where $(N_1)_{60}$ is the corrected SPT N-value

The cyclic stress ratio can be computed by:

$$\frac{\tau_{ave}}{\sigma'_o} = 0.65 \frac{a_{max}}{g} \cdot \frac{\sigma_o}{\sigma'_o} \, r_d \tag{2.15}$$

where a_{max} is the maximum acceleration at the ground surface, σ_o and σ'_o are the total overburden pressure and the initial effective overburden pressure on the sand layer under consideration and r_d is the stress reduction factor varying from a value of 1 at the ground surface to a value of 0.9 at a depth of about 10 m (30 ft) (Seed et al., 1987).

Note that T. O'Rourke et al. (1991) used a similar approach to estimate liquefaction induced settlement in the Marina District. As noted by T. O'Rourke et al., there is good agreement between the estimated and measured settlements for the natural soils and land-tipped fill, but the estimated settlements of the hydraulic fill are almost twice as much as those observed in the field.

Seed et al.'s analytical approach provides a relatively accurate estimate of ground settlement. However, it is somewhat complex and requires detailed information on site condition and soil properties.

Takada and Tanabe (1988) developed two empirical regression equations for liquefaction-induced ground settlement at embankments and plain (level) sites based on 404 observations during five Japanese earthquakes.

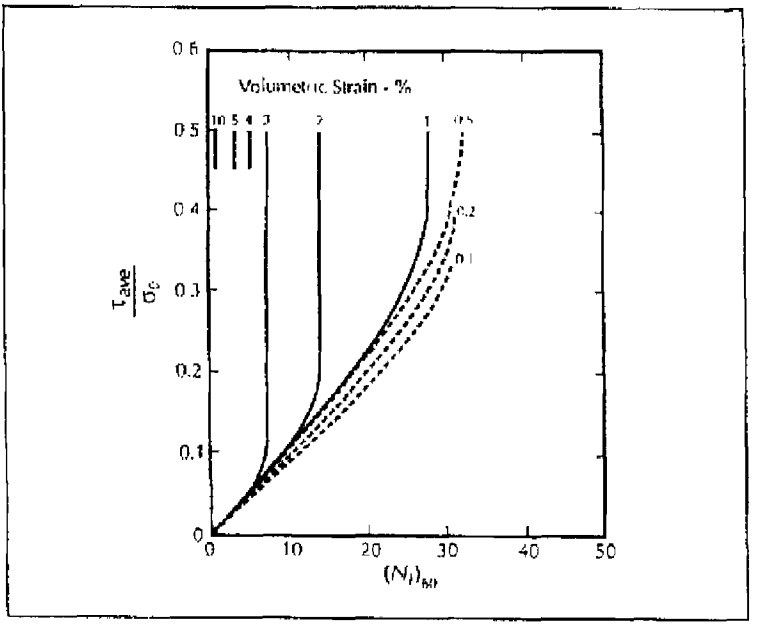

After Tokimatsu and Seed, 1987

■ Figure 2.13 Relation between Cyclic Stress Ratio, $(N_1)_{60}$ and Volumetric Strain for Saturated Sands

For embankment:

$$\delta = 0.11H_1H_2a_{max}/N+20.0 \tag{2.16}$$

For plain site:

$$\delta = 0.30H_1a_{max}/N+2.0 \tag{2.17}$$

where δ is the ground settlement in centimeters, H_1 is the thickness of saturated sand layer (in meters), H_2 is the height of embankment (in meters), N is the SPT N-value in the sandy layer, and a_{max} is the ground acceleration in gals. Takada and Tanabe's empirical approach is simple but somewhat less accurate than the Seed et al.'s approach.